

# Tri-polarised antenna – a virtual rotatable dual-polarised antenna used in polarised beampattern synthesis

ISSN 1751-8725


Received on 11th September 2014

Revised on 6th March 2015

Accepted on 10th June 2015

doi: 10.1049/iet-map.2014.0611

www.ietdl.org

Wanqiu Hu , Yongzhen Li, Mianquan Li, Siwei Chen, Xuesong Wang, Shunping Xiao

State Key Laboratory of Complex Electromagnetic Environment Effects on Electronics and Information System, National University of Defense Technology, Changsha 410073, People's Republic of China

✉ E-mail: huwanqiu1985@gmail.com

**Abstract:** Tri-polarised antennas are exploited to synthesise the optimal polarised beampattern in this study. First, the characteristics of a single tri-polarised antenna are studied with an infinite current sheet model. Using the cross-product algorithm, the authors find that three co-located orthogonal current sheets are equivalent to a pair of orthogonal current sheets in a particular orientation. It implies that the tri-polarised antenna is just virtually equivalent to a rotatable dual-polarised antenna. Then by formulating the problem in a convex form, they adopt the convex optimisation algorithm to synthesise optimal polarised beampattern of the tri-polarised array. The simulation results show that due to the increased orientation degree of freedom, the sidelobe and cross-polarisation level of tri-polarised array are significantly lower than the dual-polarised array.

## 1 Introduction

The polarised beampattern synthesis has received much attention over recent years. Several works [1–7] dealing with the joint synthesis of power pattern and polarisation have been declared in the literature. In [1], an iterative least-square method is presented to synthesise a main beam with optimised circular polarisation for conformal arrays. The ideal shape of the power pattern and the polarisation are defined as the desired radiation pattern in a least-square optimisation. An adaptive array approach is also applied in [2] to synthesise a beam with optimised polarisation employing dual-polarised patch antennas as radiators.

The aforementioned methods cannot ensure that the optimum is achieved, since the optimisation problems they solve are not transformed into convex programs. The exploitation of convexity in array synthesis problems has been introduced in [3]. Such a convex formulation has been proposed in [4] to optimally synthesise pencil beams. The approach guarantees the achievement of the global optimum using local optimisation techniques and can, moreover, deal with any convex constraint on the unknowns, such as near-field constraints.

The optimal synthesis of beampattern having any state of polarisation via convex optimisation has been addressed in [5] using an array of vector antennas. The vector array synthesis problem is cleverly transformed into a scalar one using an orthogonal transformation, which then makes the problem efficiently solvable. Later on, a method to synthesise the spatial power pattern while optimising polarisation over an angular region is proposed in [6]. Moreover, in [7], a finite-impulse response filter is set at each element to directly optimise the synthesised polarisation and wideband power patterns. Both the optimisations of the sum and difference patterns are formulated as convex programming problems to obtain efficient solutions.

In this paper, we employ the tri-polarised antennas as the array elements to synthesise the desired polarised beampattern. The tri-polarised antenna used in this paper is illustrated in Fig. 1*b*. Compared with the traditional dual-polarised antenna (Fig. 1*a*), the tri-polarised antenna add a new element orthogonal to the dual-polarised antenna plane, and the three radiators are aligned with the coordinates  $x$ ,  $y$ , and  $z$ , respectively. In wireless communications, the tri-polarised antenna increases the capacity and the robustness [8–12] of the multiple-input–multiple-output

systems and there are several designs of the tri-polarised antennas that have been proposed in [13, 14]. In the current paper, we find a new property of tri-polarised antenna: tri-polarised antenna is virtually equivalent to a rotatable dual-polarised antenna, which will explain that why the tri-polarised antenna performs better than the dual-polarised antenna. Then, we propose a convex optimisation algorithm to synthesise optimal polarised beampattern. Our results show that the maximum sidelobe level and cross-polarisation level of tri-polarised array are much lower than that of the dual-polarised array.

The rest of this paper is organised as follows. In Section 2, current distribution and the radiation characteristics of tri-polarised antenna are analysed. In Section 3, we introduce the geometric of the array and formalise the polarised waveform synthesis as the convex optimisation problem. Numerical examples are presented in Section 4 to illustrate the potentialities of the proposed array and method. The conclusions are drawn in Section 5.

## 2 Characteristics analysis of tri-polarised antenna

In this part, we consider the tri-polarised antenna composed of three infinite current sheet radiators (e.g. Hertzian dipoles) which govern the behaviour of different practical array. We assume that the three radiators are perfectly matched to their feeding transmission lines over frequency and scanning angle, and do not couple to each other.

### 2.1 Analysis of three co-located orthogonal current sheets

Let  $\mathbf{a}_r$  be a unit vector representing a spatial direction in  $\mathbb{R}^3$ . We can write  $\mathbf{a}_r$  in the form

$$\mathbf{a}_r = [\sin \theta \cos \phi, \sin \theta \sin \phi, \cos \theta]^T \quad (1)$$

where  $0 \leq \theta \leq \pi$  is the elevation angle,  $0 \leq \phi < 2\pi$  is the azimuth angle, and  $\theta$ ,  $\phi$  have been shown in Fig. 1. For each  $\mathbf{a}_r$ , we further

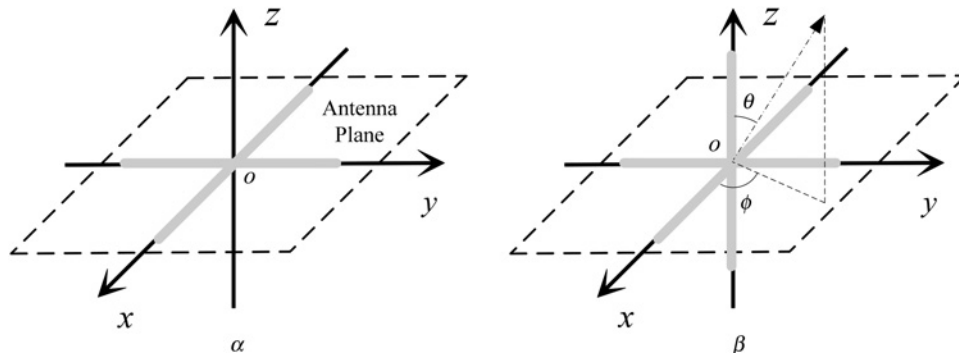


**Fig. 1** Schematic view of

a Dual-polarised antenna

b Tri-polarised antenna composed of two or three superimposed orthogonal infinite current sheet radiators

define

$$\begin{aligned} \mathbf{a}_\phi(\theta, \phi) &= \frac{1}{\sin \theta} \frac{\partial \mathbf{a}_r}{\partial \phi} = [-\sin \phi, \cos \phi, 0]^T \\ \mathbf{a}_\theta(\theta, \phi) &= \frac{\partial \mathbf{a}_r}{\partial \theta} = [\cos \theta \cos \phi, \cos \theta \sin \phi, -\sin \theta]^T \end{aligned} \quad (2)$$

We observe that  $\mathbf{a}_\theta(\theta, \phi)$ ,  $\mathbf{a}_\phi(\theta, \phi)$ ,  $\mathbf{a}_r$  forms a right-hand coordinate system.

Assuming that the  $i$ th element of the tri-polarised antenna is excited with  $w_i = |w_i| \exp(j\psi_i)$ , the current sheets can be expressed as

$$\mathbf{J}_i = w_i \mathbf{a}_i, \quad i = x, y, z \quad (3)$$

where the time harmonic factor  $\exp(j\omega t)$  is omitted.

Then, the three orthogonal current sheets satisfy the following theorem generally:

*Theorem:* Every non-zero vector  $[\mathbf{J}_x, \mathbf{J}_y, \mathbf{J}_z]^T$  has the unique representation

$$\begin{bmatrix} \mathbf{J}_x \\ \mathbf{J}_y \\ \mathbf{J}_z \end{bmatrix} = \mathbf{J}_r(\beta_0, \alpha_0), \quad (4)$$

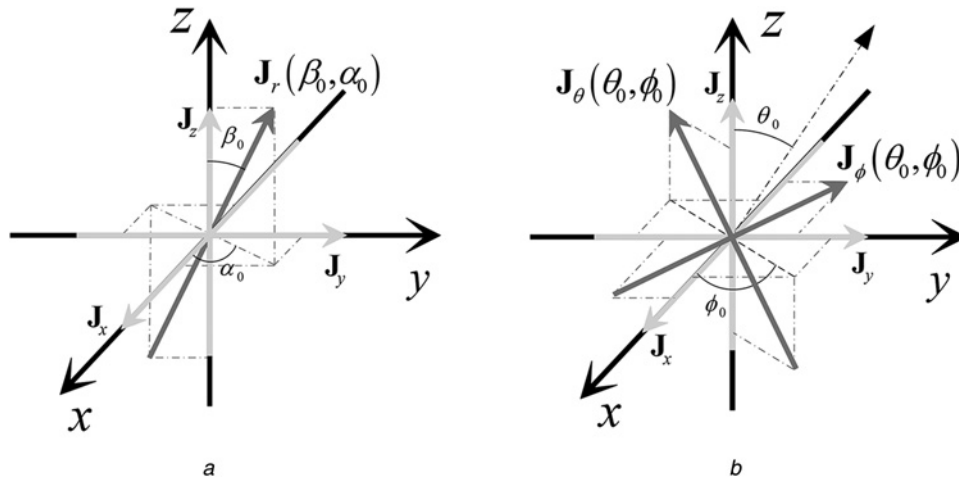


**Fig. 2** Equivalent current ( $s$ ) of the tri-polarised antenna

a Three orthogonal currents are equivalent to a single current collocated with the tri-polarised antenna

b Three orthogonal currents are equivalent to a pair of orthogonal currents collocated with the tri-polarised antenna

or

$$\begin{bmatrix} \mathbf{J}_x \\ \mathbf{J}_y \\ \mathbf{J}_z \end{bmatrix} = \mathbf{J}_\phi(\theta_0, \phi_0) + \mathbf{J}_\theta(\theta_0, \phi_0) \quad (5)$$

where

$$\mathbf{J}_r(\beta_0, \alpha_0) = w_0 \begin{bmatrix} \sin \beta_0 \cos \alpha_0 \mathbf{a}_x \\ \sin \beta_0 \sin \alpha_0 \mathbf{a}_y \\ \cos \beta_0 \mathbf{a}_z \end{bmatrix},$$

$\mathbf{J}_\phi(\theta_0, \phi_0) = w_\phi \mathbf{a}_\phi(\theta_0, \phi_0)$ ,  $\mathbf{J}_\theta(\theta_0, \phi_0) = w_\theta \mathbf{a}_\theta(\theta_0, \phi_0)$ ,  $w_\phi, w_\theta, w_0 \in \mathbb{C}$  (for proof see the Appendix).

The above theorem shows that the currents in the tri-polarised antenna with arbitrary excitations are equivalent to a single current or a pair of orthogonal currents collocated with the tri-polarised antenna, as represented in Fig. 2. If we treat (4) as the amplitude of one current in a pair of orthogonal currents in (5) is zero, then we obtain the following conclusion: three co-located orthogonal current sheets are equivalent to a pair of orthogonal current sheets in a particular orientation.

This discovery simplifies characteristic analysis of the tri-polarised antenna. We will compare the performance of the dual-polarised antenna with the tri-polarised antenna in the next section.

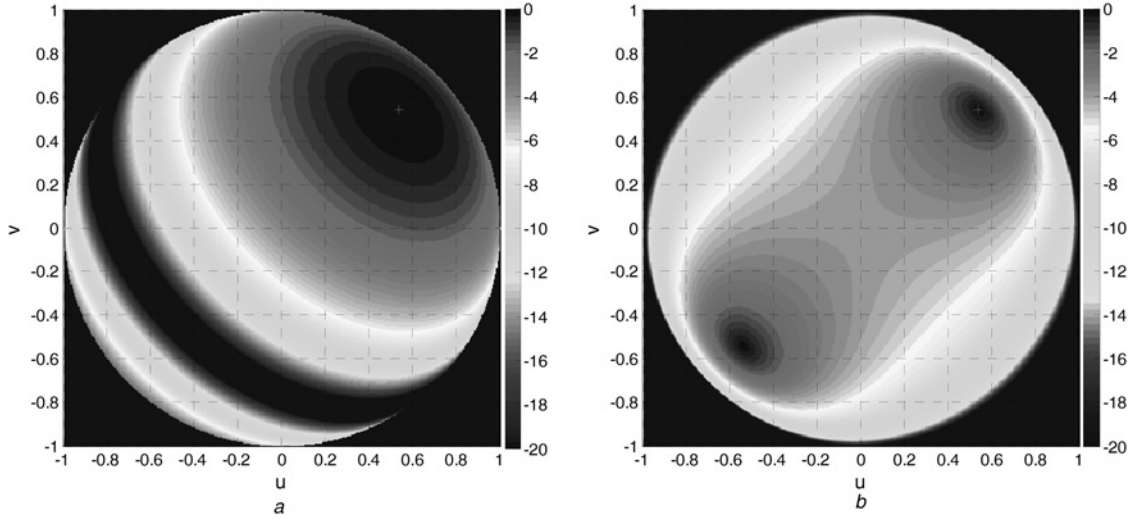


**Fig. 3** Axial ratio (in dB) for

*a* Tri-polarised antenna

*b* Dual-polarised antenna when synthesising circular polarisation at  $(\theta_0, \phi_0) = (50^\circ, 45^\circ)$ , in the upper half-space  $z > 0$ , symbol '+' indicates the scanning direction

## 2.2 Polarisation performance comparison of dual- and tri-polarised antennas

According to the above foundation, when we want tri-polarised antenna scans at the direction  $(\theta_0, \phi_0)$ , we can control the orientation of the virtual dual-polarised antenna right pointing at the scanning direction (dual-polarised antenna with optimal orientation). We can control the weights of tri-polarised antenna to virtually obtain an optimal oriented dual-polarised antenna. If the desired polarisation is left circular, then the weights of tri-polarised antenna  $\mathbf{w}_{\text{tri}}$  can be expressed as

$$\mathbf{w}_{\text{tri}} = \frac{\sqrt{2}}{2} \begin{bmatrix} -\sin \phi_0 \\ \cos \phi_0 \\ 0 \end{bmatrix} + \frac{j\sqrt{2}}{2} \begin{bmatrix} \cos \theta_0 \cos \phi_0 \\ \cos \theta_0 \sin \phi_0 \\ -\sin \theta_0 \end{bmatrix} \quad (6)$$

Fig. 3 shows the polarisation properties of the tri-polarised antenna and the dual-polarised antenna (located in the  $x$ - $y$  plane as shown in Fig. 1a) when synthesising circular polarisation at  $(\theta_0, \phi_0) = (50^\circ, 45^\circ)$ . Weights of dual-polarised antenna to synthesise the desired polarisation are the same with Boryszenko's [15].

As shown in Figs. 3a and b, the axial ratio of the tri-polarised antenna is much higher than the dual-polarised antenna in the region near the scanning direction. It implies that the axial ratio degradation of the tri-polarised antenna is much slower (versus space angle) than the dual-polarised antenna, and the polarisation purity of tri-polarised antenna is much better than dual-polarised antenna at larger scanning angles. The reason for the better performance of the tri-polarised antenna is that the tri-polarised antenna is virtually equivalent to a dual-polarised antenna with optimal orientation, whereas the dual-polarised antenna located in the  $x$ - $y$  plane works in its larger scanning angle.

## 3 Tri-polarised antenna array beam pattern synthesis

In this section, we formulate the problem of the optimal beam pattern synthesis with full polarisation control. We first introduce the configurations of the tri-polarised array used in this paper, and then formulate the beam pattern synthesis problem using tools from convex optimisation.

### 3.1 Antenna array

We consider an antenna array composed of  $N$  elements placed at known locations. The problem is described as a one-dimensional

pattern synthesis over the angle  $\theta$  in a fixed azimuth plane  $\phi = \phi_0$ . The electric field in the far field region is given by

$$\begin{aligned} \mathbf{E}(\theta) &= \sum_{n=1}^N \sum_{i=x,y,z} w_{ni} [E_{niH}(\theta) \mathbf{a}_H + E_{niV}(\theta) \mathbf{a}_V] \exp(jk \mathbf{a}_{rn} \cdot \mathbf{a}_r) \\ &\triangleq E_H(\theta) \mathbf{a}_H + E_V(\theta) \mathbf{a}_V \end{aligned} \quad (7)$$

where

$$\begin{aligned} E_H(\theta) &= \sum_{n=1}^N \sum_{i=x,y,z} w_{ni} E_{niH}(\theta) \exp(jk \mathbf{a}_{rn} \cdot \mathbf{a}_r) \\ E_V(\theta) &= \sum_{n=1}^N \sum_{i=x,y,z} w_{ni} E_{niV}(\theta) \exp(jk \mathbf{a}_{rn} \cdot \mathbf{a}_r) \end{aligned} \quad (8)$$

$E_H(\theta)$  and  $E_V(\theta)$  are the H and V components of the synthesised field, the polarisation basis is chosen as  $\mathbf{a}_H = \mathbf{a}_\phi(\theta, \phi_0)$ ,  $\mathbf{a}_V = \mathbf{a}_\theta(\theta, \phi_0)$ ,  $w_{ni}$ ,  $E_{niH}(\theta)$  and  $E_{niV}(\theta)$  are the weights, H and V polarisation response of the  $i$ th ( $i=x, y, z$ ) component of  $n$ th element, respectively,  $k$  is the free-space propagation constant,  $\mathbf{a}_{rn}$  represents the location of the  $n$ th array element.

We further introduce  $\mathbf{w}$  to be the concatenation of all  $w_{ni}$

$$\mathbf{w} = [w_{1x}, w_{1y}, w_{1z}, \dots, w_{Nx}, w_{Ny}, w_{Nz}]^T \quad (9)$$

For the extension to a conformal array, we should convert the response of each element from its local coordinate system to the global coordinate system, the details can be seen in [16]. In Section 4, we will give an example of the conformal array.

### 3.2 Optimal polarised pattern synthesis

The problem of polarised pattern synthesis is to design the antenna weights  $\mathbf{w}$  to achieve a desired pattern. Specifically, our goal is to synthesise a beam pattern with the following properties:

- (i) a main beam in the direction  $\theta_0$  with sidelobes below a given upper bound  $\tau_{\text{SL}}$  over an angular region  $\Omega_{\text{SL}}$  and
- (ii) a low cross-polarisation level, optimised over an angular region  $\Omega_p$ .

The regions  $\Omega_{\text{SL}}$  and  $\Omega_p$  can overlap.

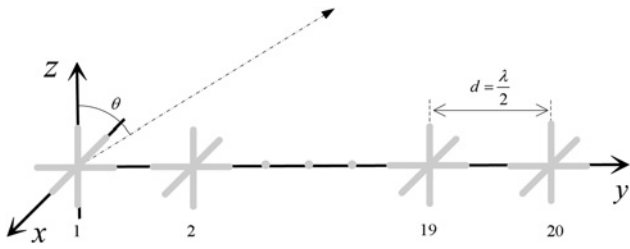


**Fig. 4** Schematic view of the linear array composed of 20 tri-polarised antennas spaced by  $\lambda/2$ . For the dual-polarised array, the dual-polarised antenna is composed with two superimposed orthogonal radiators along the  $x$ - and  $y$ -axis

The magnitude of the vector electric field is equal to

$$\|E(\theta)\|_2 = \sqrt{\|E_H(\theta)\|^2 + \|E_V(\theta)\|^2} \quad (10)$$

The sidelobes bound will be imposed on (10) over  $\Omega_{SL}$  to handle the spatial power constraint.

Let us now focus on the polarisation constraint. Given a polarisation, characterised by  $(\gamma_0, \delta_0)$ ,  $\gamma_0$  and  $\delta_0$  are the relative amplitude and phase difference between H and V components [17], can be synthesised over a range of directions in [6]. In the current paper, we notice that if we choose co-polarisation and cross-polarisation unit components  $a_{Co}$  and  $a_{Cr}$  as the polarisation basis, then we will obtain

$$E(\theta) = E_{Co}(\theta)a_{Co} + E_{Cr}(\theta)a_{Cr} \quad (11)$$

where  $E_{Co}$  and  $E_{Cr}$  are co- and cross-polarisation components of the electric field, and

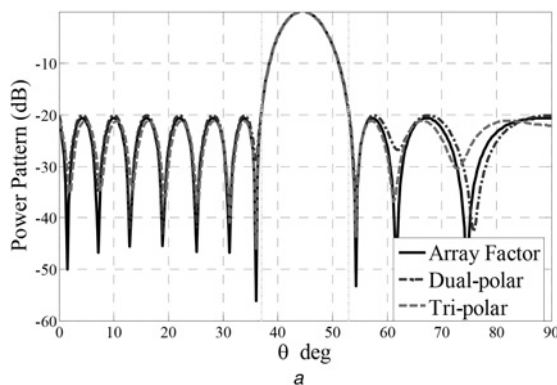
$$\begin{bmatrix} a_{Co} \\ a_{Cr} \end{bmatrix} = \begin{bmatrix} \cos \gamma_0 & \sin \gamma_0 e^{j\delta_0} \\ \sin \gamma_0 & -\cos \gamma_0 e^{j\delta_0} \end{bmatrix} \begin{bmatrix} a_H \\ a_V \end{bmatrix} \quad (12)$$

From (12), we obtain

$$\begin{bmatrix} a_H \\ a_V \end{bmatrix} = \begin{bmatrix} \cos \gamma_0 & \sin \gamma_0 \\ \sin \gamma_0 e^{-j\delta_0} & -\cos \gamma_0 e^{-j\delta_0} \end{bmatrix} \begin{bmatrix} a_{Co} \\ a_{Cr} \end{bmatrix} \quad (13)$$

Combining (7), (11) and (13), we obtain

$$\begin{bmatrix} E_{Co}(\theta) \\ E_{Cr}(\theta) \end{bmatrix} = \begin{bmatrix} \cos \gamma_0 & \sin \gamma_0 e^{-j\delta_0} \\ \sin \gamma_0 & -\cos \gamma_0 e^{-j\delta_0} \end{bmatrix} \begin{bmatrix} E_H(\theta) \\ E_V(\theta) \end{bmatrix} \quad (14)$$



Hence to optimise the polarisation we can impose

$$\|E_{Cr}(\theta)\|_2 \leq \tau_{Cr}, \quad \theta \in \Omega_P \quad (15)$$

where  $\tau_{Cr}$  is the limitation of the maximum cross-polarisation level, which allows to tune the degree of accuracy with which the desired polarisation is achieved.

Then the synthesis problem can be written as

$$\begin{aligned} \min_w \quad & \tau_{Cr} \\ \text{s.t.} \quad & E_{Co}(\theta_0) = 1 \\ & |E_{Cr}(\theta)|^2 \leq \tau_{Cr}, \quad \theta \in \Omega_P \\ & |E_{Co}(\theta)|^2 + |E_{Cr}(\theta)|^2 \leq \tau_{SL}, \quad \theta \in \Omega_{SL} \end{aligned} \quad (16)$$

It is easy to see that the above problem is a second-order cone programming (SOCP) problem. There are well-developed numerical methods to solve a general SOCP problem [18–21], such as the interior point method. In the next section, we adopt an optimisation toolbox, SeDuMi [22], to solve the SOCP formulated above.

## 4 Numerical results

In this section, numerical results are presented. Let us remind that any state of polarisation can be synthesised in (16) and (18); in the examples below, we take circular polarisation as an example to validate and illustrate the potentialities of the tri-polarised array and the proposed approach. Linear and conformal arrays are considered in the simulation.

### 4.1 Linear arrays

In this case, a linear array composed of 20 tri-polarised antennas spaced by  $\lambda/2$  is considered. A schematic view of the linear array is shown in Fig. 4. To compare with the tri-polarised antenna array, we also consider an array of 20 dual-polarised antennas with the same array structure, and the dual-polarised antenna is composed with two superimposed orthogonal radiators along  $x$ - and  $y$ -axis, respectively.

We first study the sidelobe levels of the array and do not consider the polarisation purity, then we obtain the following optimised

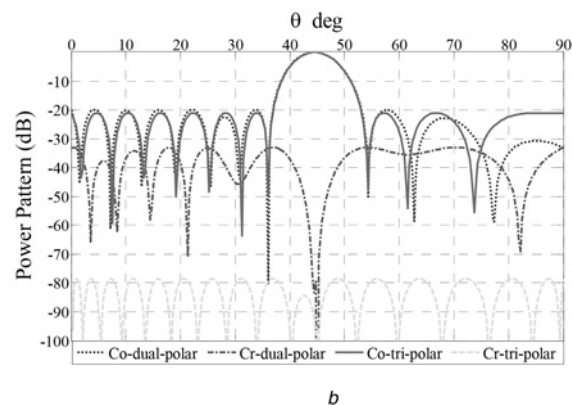


**Fig. 5** Optimised power pattern of dual- and tri-polarised array  
a Considering the sidelobe level only  
b Considering the sidelobe level and cross-polarisation level simultaneously

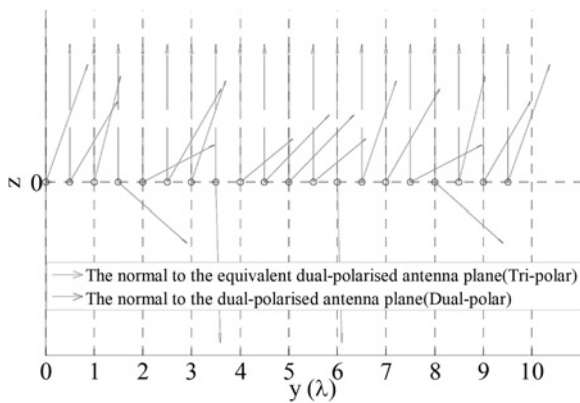


**Fig. 6** Normal to the equivalent dual-polarised antenna for tri-polarised antenna and the antenna plane of the dual-polarised antenna seen from the x-axis

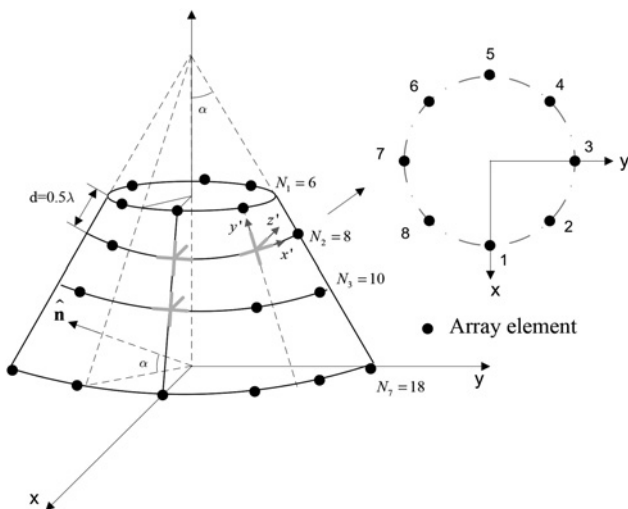


**Fig. 7** Geometry of the conformal array and the element arrangement of subarray. The tri-polarised antenna is placed along with the local coordinate  $x'$ -,  $y'$ -,  $z'$ -axis, respectively, while the dual-polarised antenna is placed along the  $x'$ -,  $y'$ -axis

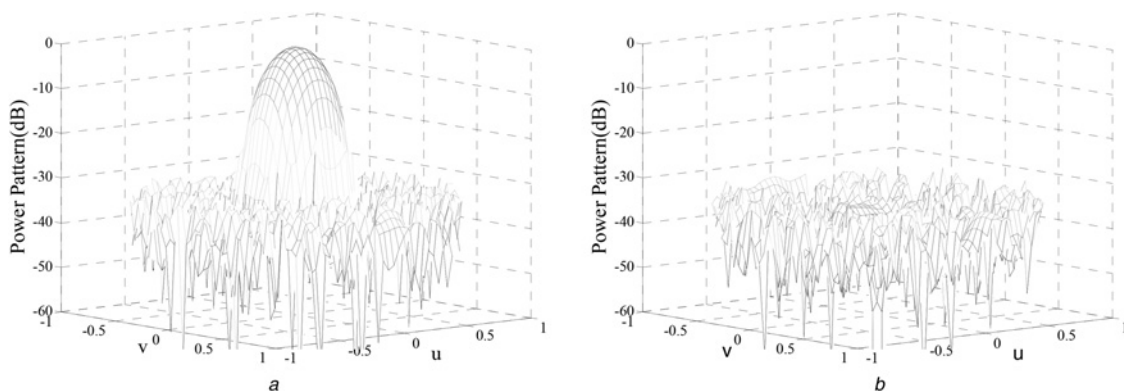


**Fig. 8** Power pattern synthesised by tri-polarised array

a Co-polarised component

b Cross-polarised component with the main beam pointing at  $(\theta_0, \phi_0) = (0^\circ, 0^\circ)$ , the maximum sidelobe level (cross-polarisation level) is  $-32.65$  dB

problem:

$$\begin{aligned} \min_w \quad & \tau_{\text{SL}} \\ \text{s.t.} \quad & E_{\text{Co}}(\theta_0) = 1 \\ & |E_{\text{Co}}(\theta)|^2 + |E_{\text{Cr}}(\theta)|^2 \leq \tau_{\text{SL}}, \quad \theta \in \Omega_{\text{SL}} \end{aligned} \quad (17)$$

In Fig. 5a, we synthesise a circular polarisation in the direction  $\theta_0 = 45^\circ$  with the optimised sidelobes over  $\Omega_{\text{SL}} = [0^\circ, 37^\circ] \cup [53^\circ, 90^\circ]$ . When we choose tri-polarised antenna as the array element, the sidelobe level is 1.1 dB lower than dual-polarised array in the current scanning angle. In other scanning angles, we obtain a similar sidelobe difference, because the sidelobe level is mainly determined by the array factor in the linear array. However, when we constrain sidelobe level below  $-20$  dB, and optimise the cross-polarisation level, we find that the cross-polarisation synthesised by the tri-polarised array is 45.3 dB lower than by the dual-polarised array over  $\Omega_p = [0^\circ, 90^\circ]$  (Fig. 5b), which establishes the good quality of the synthesised circular polarisation.

When the weights of the tri-polarised antenna are obtained, the optimised orientation and weights of the equivalent dual-polarised antenna are obtained according to Section 2. Fig. 6 shows normal to the equivalent dual-polarised antenna plane. After optimisation, normal to the rotated dual-polarised antenna has changed significantly compared with the dual-polarised antenna. We observe that exploiting tri-polarised antenna improves the polarisation purity of the array significantly.

#### 4.2 Conformal array

Fig. 3 shows the structure of the conformal array used in simulation. The dots represent possible element locations. Circular array is the building block of the array. Each concentric circle represents the intersection of a  $z = \text{constant}$  plane with the cone. Repetitive circular sub-arrays with linearly ascending diameters form a conical array. Elements around each sub-array are parallel to the  $xy$ -plane of the global coordinate system  $xyz$ .  $d$  is the distance between two adjacent sub-arrays along the cone element. In this paper, we set  $d = \lambda/2$ , where  $\lambda$  is the wavelength. The half cone angle  $\alpha$  is  $20^\circ$  and the radius of the cone's base is  $1.53\lambda$ .  $M$  circular sub-arrays with each having  $N_i$  ( $i = 1, 2, \dots, M$ ) elements at the circle perimeter form a conical array. The arc length between two adjacent elements  $d_i$  ( $i = 1, 2, \dots, M$ ) in each circular sub-array is set equal, and satisfies  $d_i \in [0.50\lambda, 0.54\lambda]$ .  $N_i$  can be determined by the constraint of  $d_i$ , and satisfies  $N_i = 4 + 2i$ ,  $i = 1, 2, \dots, M$ . In the simulation, we set  $M = 7$ .

The local coordinate system  $x'y'z'$  is defined as follows: at each element location, the  $z'$ -axis is along with the normal to the

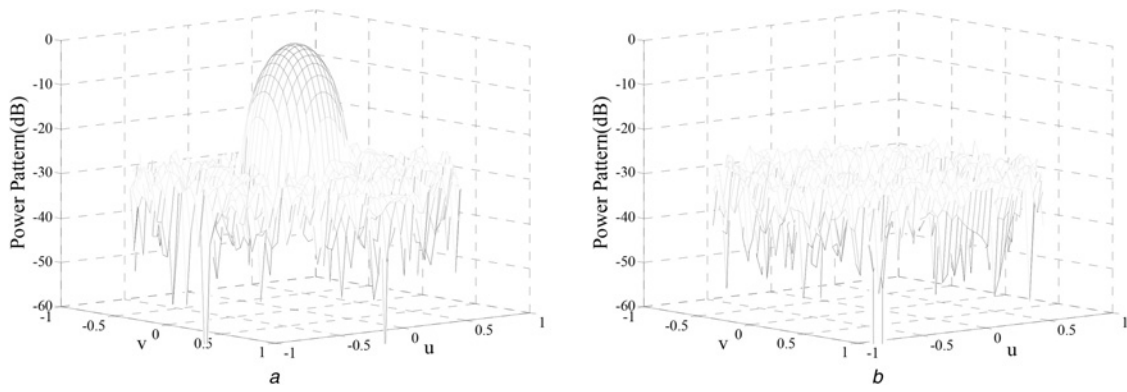


**Fig. 9** Power pattern synthesised by dual-polarised array

a Co-polarised component

b Cross-polarised component with the main beam pointing at  $(\theta_0, \phi_0) = (0^\circ, 0^\circ)$ , the maximum sidelobe level (cross-polarisation level) is  $-26.23$  dB

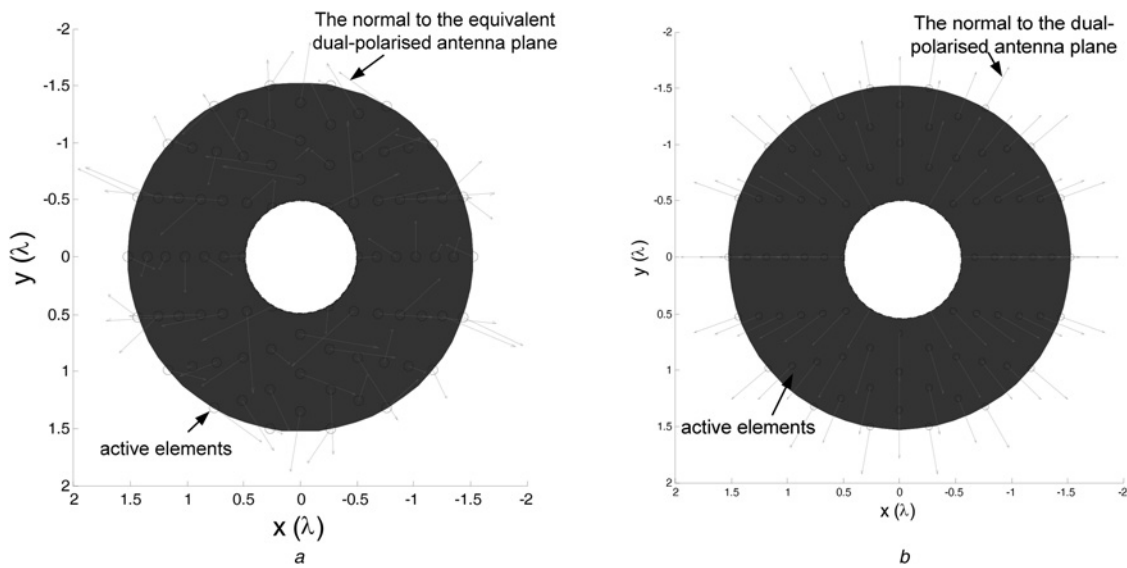


**Fig. 10** Normal to the equivalent dual-polarised antenna for tri-polarised antenna and the antenna plane of the dual-polarised antenna seen from the x-axis

surface of the cone, the  $y'$ -axis is along with the cone element (from the base to the apex), and the  $x'$ -axis is along the tangent of the sub-array circle,  $x'$ -,  $y'$ -,  $z'$ -axis form a right-hand coordinate system, see Fig. 7.

We can optimise the sidelobe level and the polarisation purity simultaneously, for example,  $\tau = \tau_{Cr} = \tau_{SL}$ , and we obtain

$$\begin{aligned}
 & \min_w \quad \tau \\
 & \text{s.t.} \\
 & E_{Co}(\theta_0, \phi_0) = 1 \\
 & |E_{Cr}(\theta, \phi)|^2 \leq \tau, \quad (\theta, \phi) \in \Omega_p \\
 & |E_{Co}(\theta, \phi)|^2 + |E_{Cr}(\theta, \phi)|^2 \leq \tau, \quad (\theta, \phi) \in \Omega_{SL}
 \end{aligned} \tag{18}$$

The optimisation algorithm returns the sidelobes level or cross-polarisation level whichever is great.

The pattern synthesised by tri-polarised array and dual-polarised array are illustrated in Figs. 8 and 9. After optimisation, the maximum sidelobe level and cross-polarised level of the tri-polarised antenna are 6.42 dB lower than the correspondences of dual-polarised antenna. The comparison between Figs. 8 and 9 implies that when we use the tri-polarised antenna, the performance of the array is improved.

Fig. 10a shows the normal to the equivalent dual-polarised antenna plane. After optimisation, normal to the equivalent dual-polarised antenna has changed significantly compared with the dual-polarised antenna Fig. 10b.

In [5] the authors point out that because the tri-polarised antenna virtually increases the array size, the power gain of the main beam (over the sidelobes) is improved compared with the dual-polarised antenna. Our work further points out that the main reason for the performance improvement is that the tri-polarised antenna increases the orientation degree of freedom of dual-polarised antenna.

## 5 Conclusion

Tri-polarised antennas are used to the polarised beampattern synthesis in this paper. From an infinite current sheet model, we find that three co-located orthogonal current sheets are equivalent to a pair of orthogonal current sheets in a particular orientation. It means that it is unnecessary to rotate the dual-polarised antenna practically, the rotation can be achieved virtually by controlling the excitation of the tri-polarised antenna. Then we propose a convex optimisation algorithm to synthesise the optimal polarised beampattern. The simulation results show that the performance (sidelobe level and cross-polarisation level) of the array is significantly improved by using the tri-polarised antenna elements.

We have obtained general conclusions of tri-polarised antenna and testified the proposed method through the theoretical analysis from the infinite current sheet model in this paper. To design an array of the tri-polarised antennas and measure the radiation patterns from a fabricated prototype is part of our future work.

## 6 Acknowledgments

This work was supported by National Science Fund for Distinguished Young Scholars of China (no. 60802078, no. 61101180, no. 41301490 and no. 61401488), China Postdoctoral Science Foundation (no. 20110490088).

## 7 References

- Vaskelainen, L.I.: 'Iterative least-squares synthesis methods for conformal array antennas with optimized polarization and frequency properties', *IEEE Trans. Antennas Propag.*, 1997, **45**, (7), pp. 1179–1185
- Dohmen, C., Odenaal, J.W., Joubert, J.: 'Synthesis of conformal arrays with optimized polarization', *IEEE Trans. Antennas Propag.*, 2007, **55**, (10), pp. 2922–2925
- Lebret, H., Boyd, S.: 'Antenna pattern synthesis via convex optimization', *IEEE Trans. Signal Process.*, 1997, **45**, (3), pp. 526–531
- Isernia, T., Iorio, P.D., Soldovieri, F.: 'An effective approach for the optimal focusing of array fields subject to arbitrary upper bounds', *IEEE Trans. Antennas Propag.*, 2000, **48**, (12), pp. 1837–1847
- Xiao, J.-J., Nehorai, A.: 'Optimal polarized beam pattern synthesis using a vector-antenna array', *IEEE Trans. Signal Process.*, 2009, **57**, (2), pp. 576–587
- Fuchs, B., Fuchs, J.J.: 'Optimal polarization synthesis of arbitrary arrays with focused power pattern', *IEEE Trans. Antennas Propag.*, 2011, **59**, (12), pp. 4512–4519
- Li, M., Chang, Y., Li, Y., et al.: 'Optimal polarised pattern synthesis of wideband arrays via convex optimization', *IET Microw., Antennas Propag.*, 2013, **7**, (15), pp. 1228–1237
- Gupta, G., Hughes, B.L., Lazzi, G.: 'On the degrees of freedom in linear array systems with tri-polarised antennas', *IEEE Trans. Wirel. Commun.*, 2008, **7**, (7), pp. 2458–2462
- Quitin, F., Oestges, C., Panahandeh, A., et al.: 'Tri-polarised MIMO systems in real-world channels: channel investigation and performance analysis', *Phys. Commun.*, 2012, **5**, pp. 308–316
- Lukama, L., Konstantinou, K., Edwards, D.J.: 'Three-branch orthogonal polarisation diversity', *Electron. Lett.*, 2001, **37**, (20), pp. 1258–1259
- Lukama, L.C., Edwards, D.J., Wain, A.: 'Application of three-branch polarisation diversity in the indoor environment', *IEE Proc., Commun.*, 2003, **150**, (5), pp. 399–403
- Mtumbuka, M.C., Edwards, D.J.: 'Investigation of tri-polarised MIMO technique', *Electron. Lett.*, 2005, **41**, (3), pp. 137–138
- Gray, D., Watanabe, T.: 'Three orthogonal polarization DRA-monopole ensemble', *Electron. Lett.*, 2003, **39**, (10), pp. 766–767
- Gallee, F.: 'Development of an isotropic sensor 2–6 GHz'. Proc. European Microwave Conf. (EuMC, 2007), Munich, Oct. 2007, pp. 91–93
- Boryszenko, A.O.: 'Polarization constraints in dual-polarized phased arrays derived from an infinite current sheet model', *IEEE Antennas Wirel. Propag. Lett.*, 2009, **8**, pp. 955–958
- Morton, T. E., Pasala, K.M.: 'Performance analysis of conformal conical arrays for airborne vehicles', *IEEE Trans. Aerosp. Electron. Syst.* 2006, **42**, (3), pp. 876–890
- Stutzman, W.L.: 'Polarization in electromagnetic systems' (Artech House, Norwood, MA, 1993)
- Boyd, S., Vandenberghe, L.: 'Convex optimization' (Cambridge University Press, Cambridge, MA, 2004)
- Lebret, H., Boyd, S.: 'Antenna array pattern synthesis via convex optimization', *IEEE Trans. Signal Process.*, 1997, **45**, (3), pp. 526–532
- Zou, L., Lasenby, J., He, Z.: 'Polarisation diversity of conformal arrays based on geometric algebra via convex optimisation', *IET Radar, Sonar Navig.*, 2012, **6**, (6), pp. 417–424
- Nai, S.E., Ser, W., Yu, Z.L., Chen, H.: 'Beam pattern synthesis for linear and planar arrays with antenna selection by convex optimization', *IEEE Trans. Antennas Propag.*, 2010, **58**, (12), pp. 3923–3930
- 'CVX: MATLAB software for disciplined convex programming', Available at <http://www.stanford.edu/~boyd/software.html>, accessed 2012
- Nehorai, A., Tichavsky, P.: 'Cross-product algorithms for source tracking using an EM vector sensor', *IEEE Trans. Signal Process.*, 1999, **SP-47**, pp. 2863–2867

## 8 Appendix Proof of theorem

For non-zero  $[\mathbf{J}_x, \mathbf{J}_y, \mathbf{J}_z]^T$ , we will prove the theorem in two situations below.

Case 1: If there exists  $i, j \in \{x, y, z\}$  satisfy  $|\psi_i - \psi_j| \neq 0$  and  $\pi, i \neq j$ , then  $[\mathbf{J}_x, \mathbf{J}_y, \mathbf{J}_z]^T$  has a unique presentation

$$\begin{bmatrix} \mathbf{J}_x \\ \mathbf{J}_y \\ \mathbf{J}_z \end{bmatrix} = \mathbf{J}_\phi(\theta_0, \phi_0) + \mathbf{J}_\theta(\theta_0, \phi_0) \quad (19)$$

where  $\mathbf{J}_\phi(\theta_0, \phi_0) = w_\phi \mathbf{a}_\phi(\theta_0, \phi_0)$ ,  $\mathbf{J}_\theta(\theta_0, \phi_0) = w_\theta \mathbf{a}_\theta(\theta_0, \phi_0)$ ,  $\varphi_0 \in [0, 2\pi)$ ,  $\theta_0 \in [0, \pi/2]$   $\{w_\phi, w_\theta\} \in \mathbb{C}^2$ .

We rewrite (19)

$$\begin{bmatrix} w_x \mathbf{a}_x \\ w_y \mathbf{a}_y \\ w_z \mathbf{a}_z \end{bmatrix} = w_\phi \begin{bmatrix} -\sin \phi_0 \mathbf{a}_x \\ \cos \phi_0 \mathbf{a}_y \\ 0 \mathbf{a}_z \end{bmatrix} + w_\theta \begin{bmatrix} \cos \theta_0 \cos \phi_0 \mathbf{a}_x \\ \cos \theta_0 \sin \phi_0 \mathbf{a}_y \\ -\sin \theta_0 \mathbf{a}_z \end{bmatrix} \quad (20)$$

The unit vector  $\mathbf{a}_i$ ,  $i = x, y, z$ , can be omitted in (20), and obtain

$$\begin{bmatrix} w_x \\ w_y \\ w_z \end{bmatrix} \triangleq \mathbf{w} = w_\phi \begin{bmatrix} -\sin \phi_0 \\ \cos \phi_0 \\ 0 \end{bmatrix} + w_\theta \begin{bmatrix} \cos \theta_0 \cos \phi_0 \\ \cos \theta_0 \sin \phi_0 \\ -\sin \theta_0 \end{bmatrix} \quad (21)$$

Using the vector cross-product algorithm [23], we can obtain  $\phi_0, \theta_0, w_\phi, w_\theta$  from (21). In fact, for  $\mathbf{w}$

$$\begin{aligned} \text{Re}(\mathbf{w}) \times \text{Im}(\mathbf{w}) &= \text{Re} \begin{bmatrix} w_x \\ w_y \\ w_z \end{bmatrix} \times \text{Im} \begin{bmatrix} w_x \\ w_y \\ w_z \end{bmatrix} \\ &= \begin{bmatrix} \text{Re} w_y \text{Im} w_z - \text{Re} w_z \text{Im} w_y \\ \text{Re} w_z \text{Im} w_x - \text{Re} w_x \text{Im} w_z \\ \text{Re} w_x \text{Im} w_y - \text{Re} w_y \text{Im} w_x \end{bmatrix} \triangleq \begin{bmatrix} s \\ t \\ u \end{bmatrix} \end{aligned} \quad (22)$$

where the symbol  $\times$  represents cross-product operation of the vector. Meanwhile for the right-hand side of (21), we obtain

$$\text{Re}(\mathbf{w}) \times \text{Im}(\mathbf{w}) = \begin{bmatrix} \sin \theta_0 \cos \phi_0 \\ \sin \theta_0 \sin \phi_0 \\ \cos \theta_0 \end{bmatrix} \begin{vmatrix} \text{Re}(w_\theta) & \text{Im}(w_\theta) \\ \text{Re}(w_\phi) & \text{Im}(w_\phi) \end{vmatrix} \quad (23)$$

Combining (23) and (22), and note that  $\theta_0 \in [0, \pi/2]$ , we obtain

$$\begin{aligned} \theta_0 &= \cos^{-1}(|u|) \\ \phi_0 &= \text{angle}(\text{sgn}(u)s + j\text{sgn}(u)t) \end{aligned} \quad (24)$$

and we further obtain

$$\begin{bmatrix} -\sin \phi_0 & \cos \theta_0 \cos \phi_0 \\ \cos \phi_0 & \cos \theta_0 \sin \phi_0 \\ 0 & -\sin \theta_0 \end{bmatrix}^T \mathbf{w} = \begin{bmatrix} w_\phi \\ w_\theta \end{bmatrix} \quad (25)$$

Then we obtain all the parameters  $\phi_0, \theta_0, w_\phi, w_\theta$  of (21), and from the above derivation process, we can find that the parameters are unique.

Case 2: If  $i, j \in \{x, y, z\}$ ,  $i \neq j$  satisfy  $|\psi_i - \psi_j| = 0$  or  $\pi$ , in the same way with case 1, we omit the unit vector,  $\mathbf{w}$  can be expressed as

$$\mathbf{w} = \begin{bmatrix} w_x \\ w_y \\ w_z \end{bmatrix} = \|\mathbf{w}\| \exp(j\psi_z) \begin{bmatrix} \exp[j(\psi_x - \psi_z)] \frac{|w_x|}{\|\mathbf{w}\|} \\ \exp[j(\psi_y - \psi_z)] \frac{|w_y|}{\|\mathbf{w}\|} \\ \frac{|w_z|}{\|\mathbf{w}\|} \end{bmatrix} \quad (26)$$

for  $|\psi_x - \psi_z| = 0, \pi$  and  $|\psi_y - \psi_z| = 0, \pi$  then  $\exp[j(\psi_x - \psi_z)] = \pm 1$ ,

$\exp[j(\psi_y - \psi_z)] = \pm 1$ , so. We obtain

$$\beta_0 = \cos^{-1} \frac{|w_z|}{\|\mathbf{w}\|}$$
$$\gamma_0 = \text{angle} \left( \exp[j(\psi_x - \psi_z)] \frac{|w_x|}{\|\mathbf{w}\|} + j \exp[j(\psi_y - \psi_z)] \frac{|w_y|}{\|\mathbf{w}\|} \right) \quad (27)$$

and we obtain

$$\mathbf{w} = \|\mathbf{w}\| \exp(j\phi) \begin{bmatrix} \sin \beta_0 \cos \gamma_0 \\ \sin \beta_0 \sin \gamma_0 \\ \cos \beta_0 \end{bmatrix} \quad (28)$$

Moreover,  $\beta_0$  and  $\gamma_0$  are unique from the above derivation.



Copyright of IET Microwaves, Antennas & Propagation is the property of Institution of Engineering & Technology and its content may not be copied or emailed to multiple sites or posted to a listserv without the copyright holder's express written permission. However, users may print, download, or email articles for individual use.